

不同结构钽酸钠的制备及其光解水析氢性能

黄浪欢*, 产启中, 张斌, 吴晓婧, 高鹏, 焦自斌, 刘应亮

暨南大学化学系, 广东广州 510632

摘要: 采用不同钠源, 在水热条件下实现了钙钛矿结构 NaTaO_3 、烧绿石结构 $\text{Na}_2\text{Ta}_2\text{O}_6$ 以及 $\text{NaTaO}_3/\text{Na}_2\text{Ta}_2\text{O}_6$ 异质结型复合光催化剂的可控合成, 利用 X 射线衍射、扫描电镜、高分辨透射电镜、紫外-可见漫反射光谱、荧光光谱和 X 射线光电子能谱对样品进行了表征, 探讨了钠源对所得钽酸钠样品结构的影响. 光解水析氢实验结果表明, 各钽酸盐的光催化活性顺序为 $\text{NaTaO}_3/\text{Na}_2\text{Ta}_2\text{O}_6 > \text{NaTaO}_3 > \text{Na}_2\text{Ta}_2\text{O}_6$. NaTaO_3 与 $\text{Na}_2\text{Ta}_2\text{O}_6$ 间形成的纳米尺度异质结有效抑制了光生电子和空穴的复合, 这是其具有最高光解水析氢活性的主要原因.

关键词: 光催化; 光解水; 钽酸钠; 异质结; 水热合成法

中图分类号: O643 **文献标识码:** A

收稿日期: 2011-07-29. 接受日期: 2011-09-13.

*通讯联系人. 电话: (020)85220597; 传真: (020)85221813; 电子信箱: thuangleh@jnu.edu.cn

基金来源: 国家自然科学基金 (20801023); 暨南大学青年基金 (51208024); 本科生国家创新工程 (51023031).

本文的英文电子版(国际版)由Elsevier出版社在ScienceDirect上出版(<http://www.sciencedirect.com/science/journal/18722067>).

Preparation of Sodium Tantalate with Different Structures and Its Photocatalytic Activity for H_2 Evolution from Water Splitting

HUANG Langhuan*, CHAN Qizhong, ZHANG Bin, WU Xiaojing, GAO Peng,
JIAO Zibin, LIU Yingliang

Department of Chemistry, Jinan University, Guangzhou 510632, Guangdong, China

Abstract: Sodium tantalate photocatalysts with a perovskite structure (NaTaO_3), a pyrochlore structure ($\text{Na}_2\text{Ta}_2\text{O}_6$), and a nano-heterojunction ($\text{NaTaO}_3/\text{Na}_2\text{Ta}_2\text{O}_6$) structure were controllably synthesized using the hydrothermal method. Sodium carbonate, sodium stearate, and sodium acetate were used as precursors, respectively. The physical properties of the as-prepared samples were characterized by X-ray diffraction, scanning electron microscopy, high resolution transmission electron microscopy, ultraviolet visible diffuse reflectance spectroscopy, X-ray photoelectron spectroscopy, and photoluminescence spectroscopy. The effects of the sodium precursor on the structure of sodium tantalate are discussed. The photocatalytic results indicated that the activity for the H_2 evolution half-reaction from water splitting was in the following order: $\text{NaTaO}_3/\text{Na}_2\text{Ta}_2\text{O}_6 > \text{NaTaO}_3 > \text{Na}_2\text{Ta}_2\text{O}_6$. The highest photocatalytic activity of $\text{NaTaO}_3/\text{Na}_2\text{Ta}_2\text{O}_6$ can be attributed to heterojunction formation within the nanoparticles, which significantly enhanced the separation of the electron-hole pairs.

Key words: photocatalysis; photocatalytic water splitting; sodium tantalate; heterojunction; hydrothermal synthesis

Received 29 July 2011. Accepted 13 September 2011.

*Corresponding author. Tel: +86-20-85220597; Fax: +86-20-85221813; E-mail: thuangleh@jnu.edu.cn

This work was supported by the National Natural Science Foundation of China (20801023), the Youth Fund of Jinan University (51208024), and the Undergraduate of National Innovation Project (51023031).

English edition available online at Elsevier ScienceDirect (<http://www.sciencedirect.com/science/journal/18722067>).

氢能是解决能源危机和环境问题的理想途径之一. 自从 Fujishima 等^[1]于 1972 年首次发现在近紫外光作用下, TiO_2 -Pt 电极能使水在常温下分解为

H_2 和 O_2 以来, 人们逐渐认识到光催化分解水制氢的可行性及重要性. 近年来, 光催化分解水制氢处于一个十分活跃的发展时期, 尤其在开发具有高量

子产率的新型光催化剂方面一直比较活跃. 1998年, Kudo 等^[2,3]发现, MTaO_3 ($M = \text{Li, Na, K}$) 在紫外光下分解水的效果非常显著, 在有助剂 NiO 存在的条件下, 分解纯水产生氢和氧的量子效率达到 28%. 随后, 有关钽酸盐光催化剂的制备和改性方面的研究日益受到重视, 目前报道有 MTaO_3 ($M = \text{Li, Na, K}$), M_3TaO_7 ($M = \text{Y, Yb, Gd, La}$), $\text{Ca}_2\text{Ta}_2\text{O}_7$, $\text{K}_3\text{Ta}_3\text{B}_2\text{O}_{12}$, MTa_2O_6 ($M = \text{Sr, Ba, Ni, Mn, Co}$), Bi_2MTaO_7 ($M = \text{La, Y}$), $\text{Ba}_2\text{LnTi}_2\text{Ta}_3\text{O}_{15}$ ($\text{Ln} = \text{Y, La}$), $\text{K}_2\text{Sr}_{1.5}\text{Ta}_3\text{O}_{10}$, $\text{M}_2\text{La}_{2/3}\text{Ta}_2\text{O}_7$ ($M = \text{H, K}$), $\text{ABi}_2\text{Ta}_2\text{O}_9$ ($A = \text{Ca, Sr, Ba}$), $\text{M}_5\text{Ta}_4\text{O}_{15}$ ($M = \text{Sr, Ba}$) 和 $\text{H}_2\text{SrTa}_2\text{O}_7$ 等^[4~15]. 本课题组亦曾采用固相反应结合水热法制备了具有特殊棒状结构及较高活性的新型光催化剂 $\text{Na}_2\text{Ta}_2\text{O}_6$ ^[16].

Ishihara 等^[17]曾用不同方法制备了具有烧绿石结构的 $\text{K}_2\text{Ta}_2\text{O}_6$ 及具有钙钛矿结构的 KTaO_3 , 结果表明光催化分解水活性次序为: KTaO_3 (固相反应) $< \text{KTaO}_3$ (醇盐水解) $\ll \text{K}_2\text{Ta}_2\text{O}_6$ (醇盐水解). 这是由于 TaO_6^{7-} 八面体的连接方式不同, 电子带结构亦不同, 从而导致光催化活性不同. 钽酸钠亦存在钙钛矿结构 NaTaO_3 和烧绿石结构 $\text{Na}_2\text{Ta}_2\text{O}_6$ 两种不同晶体结构. 然而到目前为止, 尚未见 NaTaO_3 和 $\text{Na}_2\text{Ta}_2\text{O}_6$ 的结构和性能上的差别报道. 可以预料, 二者虽具有相同的原子组成, 但晶体结构的差别也会导致光催化活性的不同.

本文分别以碳酸钠、硬脂酸钠和醋酸钠为钠源, 合成了钙钛矿结构 NaTaO_3 , 烧绿石结构 $\text{Na}_2\text{Ta}_2\text{O}_6$ 以及 $\text{NaTaO}_3/\text{Na}_2\text{Ta}_2\text{O}_6$ 异质结型复合光催化剂, 研究了不同结构钽酸盐的形成原因及光催化性能的差异, 并探讨了导致光催化性能差异的结构原因.

1 实验部分

1.1 钽酸盐的制备

分别称取一定量的 Ta_2O_5 (99.99%, 上海阿拉丁试剂有限公司) 置于烧杯中, 按照 Ta 与 Na 摩尔比为 1:3 分别称取无水碳酸钠、硬脂酸钠和醋酸钠 (AR, 均为广州化学试剂厂), 加入 5 ml 乙二醇 (AR, 广州化学试剂厂) 及 25 ml 去离子水, 放在恒温水浴锅上 80 °C 搅拌 2 h, 装入 50 ml 聚四氟乙烯内衬的反应釜中, 放入烘箱中在 180 °C 反应 24 h, 然后自然冷却至室温, 将所得样品进行抽滤, 用去离子水洗涤产物数次直至洗净杂质离子, 在室温下自然干燥,

即得钽酸盐样品. 将所得的样品浸渍在 $\text{Ni}(\text{NO}_3)_2$ 溶液中, 连续搅拌 4 h, 将混合物高温煅烧, 即得负载 NiO 的样品.

1.2 样品的表征

运用 MSAL-XRD2 型 X 射线粉末衍射仪 (XRD) 分析样品晶相, $\text{Cu K}\alpha_1$ 辐射源 ($\lambda = 0.154056$ nm), 扫描范围 $2\theta = 10^\circ \sim 80^\circ$, 操作电压 40 kV, 电流 20 mA, 扫描速度 $4^\circ/\text{min}$. 运用 Philips XL-30 型扫描电子显微镜 (SEM) 及 JEOL-2100F 型高分辨透射电镜 (HRTEM) 观察样品形貌. 样品的紫外可见漫反射光谱 (UV-Vis DRS) 在 Shimadzu UV-2501PC 型光谱仪上测试. 样品的荧光光谱 (PL) 在 Hitachi F-4500 型荧光发射光谱仪上测试. X 射线光电子能谱 (XPS) 由 Thermo Electron ESCA LAB-250 型光电子能谱仪测定, 辐射源为 $\text{Al K}\alpha$.

1.3 光催化分解水析氢反应

光催化分解水析氢实验在光催化反应系统 (CEL-HX300, 北京中教金源科技有限公司) 中进行. 500 W 氙灯为光源, 准确称取 0.1 g 催化剂样品置于反应系统中, 由于 S^{2-} 和 SO_3^{2-} 清除空穴的能力较强, 故加入 100 ml 0.1 mol/L Na_2S 和 0.04 mol/L Na_2SO_3 的混合液作为牺牲剂^[18], 通 N_2 吹扫 30 min 后, 在磁力搅拌下连续光照反应 6 h. 通过气相色谱仪 (GC9800, 上海科创色谱仪器有限公司) 定时从反应器中采集气体样品, 分析其 H_2 含量.

2 结果与讨论

2.1 XRD 结果

图 1 为不同钽酸钠样品的 XRD 谱. 由图可见, 以 Na_2CO_3 为 Na 源所得样品为 NaTaO_3 , 为晶胞参数略有畸变的单斜晶系 (JCPDS 74-2477; $a = 0.3889$ nm, $b = 0.38885$ nm, $c = 0.3899$ nm, $\alpha = \gamma = 90^\circ$, $\beta = 90.367^\circ$), 具有 ABO_3 钙钛矿晶体结构. 而以硬脂酸钠为钠源时, 所得样品为 $\text{Na}_2\text{Ta}_2\text{O}_6$ (JCPDS 70-1155; $a = b = c = 1.044$ nm, $\alpha = \beta = \gamma = 90^\circ$), 具有与烧绿石相似的晶体结构. 当以醋酸钠为钠源时, 所得样品于 $2\theta = 22.85^\circ, 32.55^\circ, 40.23^\circ, 46.67^\circ, 52.58^\circ, 73.06^\circ$ 和 77.56° 处出现了 NaTaO_3 的特征峰, 同时在 $2\theta = 14.68^\circ, 28.32^\circ, 29.61^\circ, 34.32^\circ, 37.514^\circ, 45.08^\circ, 49.33^\circ, 51.75^\circ, 61.47^\circ, 63.58^\circ$ 和 80.05° 处出现了 $\text{Na}_2\text{Ta}_2\text{O}_6$ 的特征峰. 另外, 二者部分衍射峰和

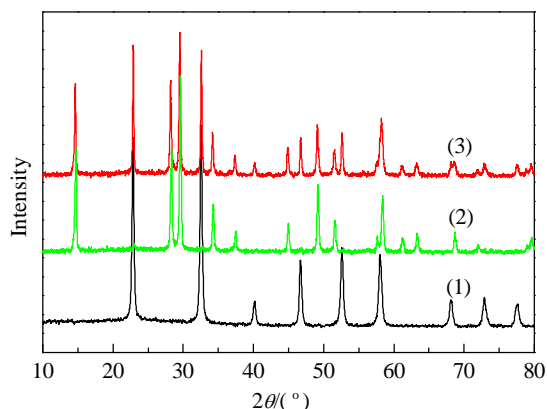


图 1 以不同钠源制得的钽酸钠样品的 XRD 谱

Fig. 1. XRD patterns of the sodium tantalate samples prepared using sodium carbonate (1), sodium stearate (2), and sodium acetate (3) as a precursor.

位置极为相近。可见，以醋酸钠为钠源制得的是复合型光催化剂 $\text{NaTaO}_3/\text{Na}_2\text{Ta}_2\text{O}_6$ 。

研究表明，高碱度条件下有利于 NaTaO_3 的生成，低碱度条件下有利于 $\text{Na}_2\text{Ta}_2\text{O}_6$ 的生成，后者为热力学介稳相，而前者则为热力学稳定相^[19]。本文结果表明，当以水溶液碱度最高的碳酸钠及碱度较低的硬脂酸钠为钠源时，分别生成 NaTaO_3 及 $\text{Na}_2\text{Ta}_2\text{O}_6$ ，与文献报道一致；但以碱度最低的醋酸钠水溶液为钠源时，所得的样品为 $\text{NaTaO}_3/\text{Na}_2\text{Ta}_2\text{O}_6$ 。我们认为，不同结构钽酸盐的生成除与 pH 有关外，还与钠源的酸根离子密切相关。这是因为采用水热法制备钽酸盐时，在高温高压下 Ta_2O_5 溶于碱性溶液，生成 TaO_6^{7-} 八面体结构单元，它在不同条件下以不同共点形式连接形成网络结构，同时 Na^+ 进入空隙位：



因此，在水热条件下不同晶相结构钽酸盐的生成取决于 TaO_6^{7-} 八面体的结合和 Na^+ 的扩散。以硬

脂酸钠为钠源时，半径大的硬脂酸根离子在 Na^+ 周围形成离子氛并与其一起移动，相应增大 Na^+ 体积，需要占据较大体积空隙，同时，硬脂酸根较难挥发，从而阻止亚稳态的 $\text{Na}_2\text{Ta}_2\text{O}_6$ 向稳态 NaTaO_3 的晶相转变，故倾向于得到原子堆积较为松散的 $\text{Na}_2\text{Ta}_2\text{O}_6$ 。当以碳酸钠为钠源时，碳酸根半径小、且水溶液碱度高，故倾向于得到原子堆积较为紧密的 NaTaO_3 。当以醋酸钠为钠源时，醋酸根离子半径介于硬脂酸根和碳酸根之间，对 Na^+ 迁移的影响亦介于二者之间，故倾向于得到具有复合结构的 $\text{NaTaO}_3/\text{Na}_2\text{Ta}_2\text{O}_6$ 。

文献报道认为，利用水热法制备碱金属钽酸盐通常需非常高的碱度^[19,20]。而本文在较低碱度下能成功制得钽酸盐，可能与乙二醇的加入有关。这是由于单纯水溶液中水分子自身的氢键作用，对 OH^- 有很强的溶剂化作用， OH^- 会被水分子屏蔽使得实际活度降低^[21]。而在水/乙二醇混合溶剂体系中，乙二醇分子体积大，对 OH^- 的溶剂化效应比水要弱许多，因此相同碱度下， OH^- 活度比水溶液中的高，因而反应活性更高，也就是说，加入乙二醇和提高溶液碱度的效果是一致的。

2.2 SEM 及 HRTEM 结果

图 2 为各钽酸钠样品的 SEM 照片。由图可见， NaTaO_3 为不规则的纳米晶，颗粒尺寸较大，多介于 500~600 nm； $\text{Na}_2\text{Ta}_2\text{O}_6$ 的尺寸较小，约 200 nm 左右，此外还生成了一些长棒状颗粒，这种棒状结构与我们前期结果^[16]一致。 $\text{NaTaO}_3/\text{Na}_2\text{Ta}_2\text{O}_6$ 的形貌与 NaTaO_3 类似，只是颗粒尺寸更小，约 300 nm 左右。水热条件下，纳米颗粒的生长机理较为复杂，颗粒的生长动力学因钠源物质、溶剂或 pH 的不同而不同，因为这些参数会影响溶液浓度、粘度，进而影响晶体生长过程中所涉及到的能量。以碳酸钠为钠源时，体系碱度高， Ta_2O_5 充分溶解，体系很快达到过饱和析晶，析出的大量晶核在进一步生长过程中受较易

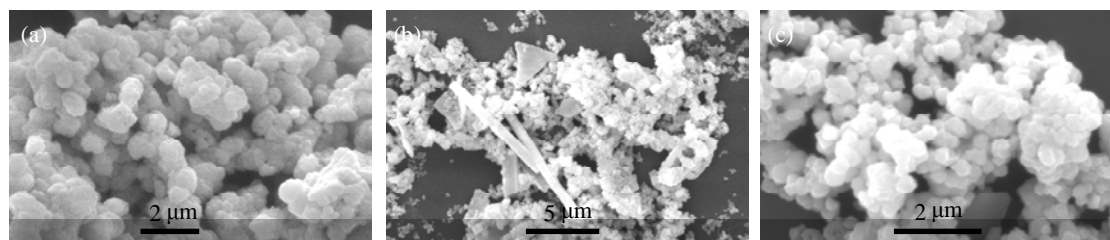


图 2 各钽酸钠样品的 SEM 照片

Fig. 2. SEM images of NaTaO_3 (a), $\text{Na}_2\text{Ta}_2\text{O}_6$ (b), and $\text{NaTaO}_3/\text{Na}_2\text{Ta}_2\text{O}_6$ (c).

去除的碳酸根离子的影响较小, 熟化过程充分, 故得到粒度相对较大的 NaTaO_3 颗粒. 以醋酸钠为钠源时, 体系碱度较低, Ta_2O_5 溶解不充分, 体系需较长时间才能达到过饱和析晶, 故得到粒度相对较小的钽酸钠颗粒. 以硬脂酸钠为钠源时, 长链状硬脂酸根较难去除, 而晶核的生长又必然伴随着溶剂的去除及基元颗粒之间化学键的形成, 故晶相转变及晶粒生长均受到抑制, 得到的是颗粒尺寸相对最小的 $\text{Na}_2\text{Ta}_2\text{O}_6$; 又由于硬脂酸根的模板作用, 部分生长基元沿着一个维度聚集, 从而得到特殊棒状结构. 结果表明, 钠源酸根离子不但影响产物晶形结构, 也因为影响成核及晶核生长速度进而影响产物形貌.

图 3 为 $\text{NaTaO}_3/\text{Na}_2\text{Ta}_2\text{O}_6$ 的 HRTEM 照片. 由图可见, NaTaO_3 纳米颗粒在 (100) 晶面的晶格间距为 0.39 nm, $\text{Na}_2\text{Ta}_2\text{O}_6$ 纳米颗粒在 (222) 晶面的晶格间距为 0.30 nm. NaTaO_3 和 $\text{Na}_2\text{Ta}_2\text{O}_6$ 纳米颗粒的晶格条纹在界面处是贯通的, 说明它们在界面处形成化学键及异质结结构. 可见 NaTaO_3 和 $\text{Na}_2\text{Ta}_2\text{O}_6$ 间具有良好的界面接触, 这有利于光催化过程中光生载流子的高效分离.

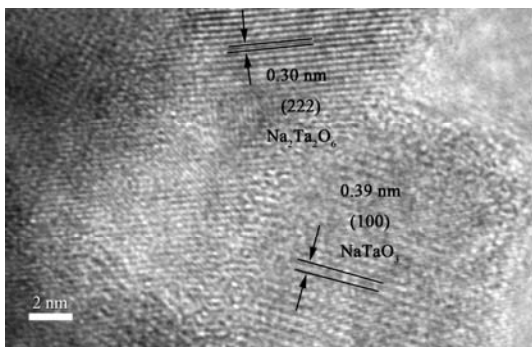


图 3 $\text{NaTaO}_3/\text{Na}_2\text{Ta}_2\text{O}_6$ 的 HRTEM 照片

Fig. 3. HRTEM image of $\text{NaTaO}_3/\text{Na}_2\text{Ta}_2\text{O}_6$.

2.3 UV-Vis DRS 结果

图 4 是各钽酸钠样品的 UV-Vis 谱. 根据公式 $E_g(\text{eV}) = 1240/\lambda(\text{nm})$ 可算出各样品的禁带宽度, 式中 λ 为吸收带边对应的波长, 其值可由吸收带边上升的拐点来确定. 经计算, NaTaO_3 , $\text{Na}_2\text{Ta}_2\text{O}_6$ 及 $\text{NaTaO}_3/\text{Na}_2\text{Ta}_2\text{O}_6$ 的带宽分别为 4.27, 4.42 及 4.13 eV. 钽酸钠价带及导带分别由 O 2p 及 Ta 5d 构成^[3,14,22]. 各样品带宽不同是因为 Ta-O 键的键长及 TaO 八面体连接方式不同. NaTaO_3 及 $\text{Na}_2\text{Ta}_2\text{O}_6$ 中, Ta-O 键键长分别为 197.8 和 199.3 pm, $\text{Na}_2\text{Ta}_2\text{O}_6$ 中

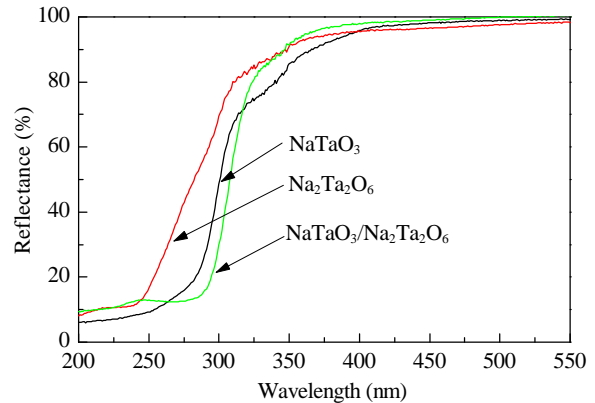


图 4 不同钽酸钠样品的 UV-Vis 光谱

Fig. 4. UV-Vis DRS spectra of different sodium tantalate samples.

较长的 Ta-O 键致使 Ta 5d 能级更高, 故其带宽较 NaTaO_3 大. $\text{NaTaO}_3/\text{Na}_2\text{Ta}_2\text{O}_6$ 带宽最小, 可能与晶体结构扭曲有关. 虽然 NaTaO_3 及 $\text{Na}_2\text{Ta}_2\text{O}_6$ 的结构单元均是 TaO_6 八面体, 但连接方式不一样, 前者为典型钙钛矿结构, 后者则为烧绿石结构, 二者形成异质结复合材料时, 界面处 TaO_6 八面体严重扭曲, 从而使能带结构发生比较复杂的变化.

2.4 PL 结果

图 5 为各钽酸钠样品在 300 nm 发射下测得的 PL 谱. PL 分析是研究半导体中载流子诱捕、迁移、传递效率及电子-空穴对再复合情况的有效手段. 研究表明^[23-27], PL 谱中相应峰高降低表明相应的氧或金属空位降低, 即材料中的复合中心减少, 从而促进光生电子和空穴的分离, 有助于提高光催化活性. 由图 5 可见, 不同样品的 PL 发射峰位置一致, 说明晶相结构的改变并未引起新的发光现象. 各样品的 PL 信号强度顺序为 $\text{Na}_2\text{Ta}_2\text{O}_6 > \text{NaTaO}_3 > \text{NaTaO}_3/\text{Na}_2\text{Ta}_2\text{O}_6$.

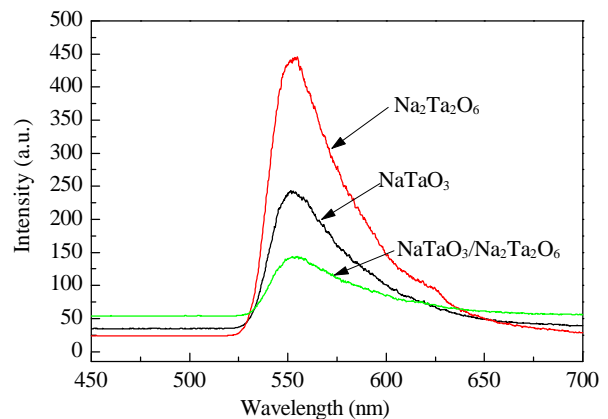


图 5 不同钽酸钠样品的荧光光谱

Fig. 5. PL spectra of different sodium tantalate samples.

TaO₃/Na₂Ta₂O₆, 在 550 nm 处样品 NaTaO₃/Na₂Ta₂O₆ 的特征发射峰强最弱, 说明其光生电子及空穴的再复合率最低, 量子效率相对最高. 研究表明^[28,29], 在相同反应条件下, 样品的光催化活性与其 PL 谱强度成正比, 这与下文结果一致.

2.5 XPS 结果

表 1 为各钽酸钠样品晶格氧的 O 1s 及 Ta 4f_{7/2} 峰结合能数据. 分析认为, Na₂Ta₂O₆ 中 TaO₆⁷⁻ 为扭曲八面体, 结构中 O 经常缺失, 同时有准自由电子产生以保持整个晶体的电中性, 这就要求 Ta⁵⁺ 接纳电子, 相应的 Ta⁵⁺ 周围电子密度增加, 屏蔽效应升高, 故 Na₂Ta₂O₆ 中 O 1s 及 Ta 4f_{7/2} 的结合能均比 NaTaO₃ 低. NaTaO₃/Na₂Ta₂O₆ 中, 在 NaTaO₃ 和 Na₂Ta₂O₆ 界面处形成的异质结结构, 有可能成为电子转移通道 (电子转移路径为 Na₂Ta₂O₆→NaTaO₃), 从而使因 O 缺失而富余准自由电子的 Na₂Ta₂O₆ 的电子密度下降, 屏蔽效应相应降低, 故 NaTaO₃/Na₂Ta₂O₆ 中 O 1s 及 Ta 4f_{7/2} 的结合能介于 NaTaO₃ 与 Na₂Ta₂O₆ 之间.

表 1 各钽酸钠样品的 O 1s 及 Ta 4f_{7/2} 结合能数据

Table 1 The binding energy of O 1s and Ta 4f_{7/2} for different samples

Sample	Binding energy (eV)	
	O 1s	Ta 4f _{7/2}
NaTaO ₃	530.1	25.8
Na ₂ Ta ₂ O ₆	529.6	24.8
NaTaO ₃ /Na ₂ Ta ₂ O ₆	529.95	25.54

2.6 各样品光催化分解水析氢性能

图 6 为紫外光下各钽酸钠样品光催化分解水析氢半反应的活性. 由图可见, 各样品析氢速率没有随反应进行而明显衰减, 表明光催化剂具有良好的稳定性. 其中 NaTaO₃/Na₂Ta₂O₆ 的析氢性能最优, 其析氢速率为 49 μmol/h, 分别是 NaTaO₃ 的 1.5 倍及 Na₂Ta₂O₆ 的 3 倍. 结合 PL 结果, 可认为光生电子及空穴的分离效率是造成上述各样品光催化活性差异的主要原因. 复合光催化剂中良好结合的纳米尺度的异质结, 可促进光生载流子的有效分离. Scaife^[30] 曾报道使用公式 $V_{fb}(NHE) = 2.94 - E_g$ 可粗略计算不含半充满 d 电子氧化物的平带电位, 式中 V_{fb} 为平带电位, 费米能级: NaTaO₃ 为 -1.33 eV, Na₂Ta₂O₆ 为 -1.48 eV, NaTaO₃/Na₂Ta₂O₆ 为 -1.18 eV. 当 NaTaO₃ 与 Na₂Ta₂O₆ 紧密接触形成异质结时, 由于 Na₂Ta₂O₆

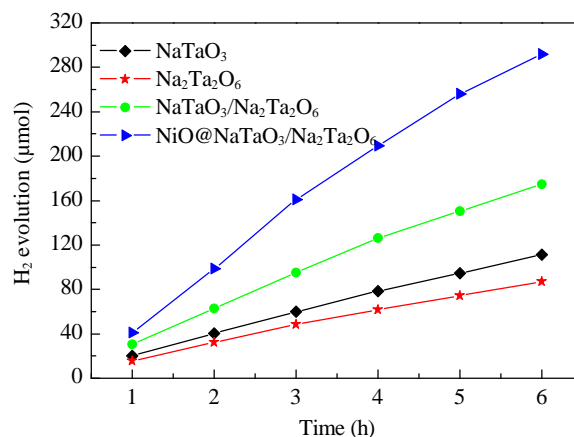


图 6 各钽酸钠样品光催化分解水还原半反应的析氢实验结果

Fig. 6. Photocatalytic activity of the sodium tantalate samples during water splitting.

费米能级比 NaTaO₃ 的高, 电子将从 Na₂Ta₂O₆ 流向 NaTaO₃^[31-33], 从而在 Na₂Ta₂O₆ 一边形成耗尽层, 在 NaTaO₃ 一边形成电子累积层, 这样在二者接触界面处形成内建电场, 其方向由 Na₂Ta₂O₆ 指向 NaTaO₃. NaTaO₃/Na₂Ta₂O₆ 光催化剂受光辐照产生光生电荷时, 光生电子逆着内建电场方向运动, 光生空穴顺着内建电场方向运动, 故异质结的内建电场能够有效抑制光致电荷复合, 提高量子效率.

结果表明, 负载 2.5% NiO 后, NaTaO₃/Na₂Ta₂O₆ 光解水析氢速率可提高将近 1.4 倍, 其反应条件尚需进一步优化. 需要指出的是, 理论上带隙越宽, 导带位置越负, 导带上被激发电子的还原能力更强, 而本文中各样品光解水析氢活性与带隙宽度并不一致, 说明能带结构并不是影响其活性的主要因素.

3 结论

研究了钠源酸根离子对所制钽酸钠样品晶相及形貌的影响, 其中以 NaAc 为 Na 源制得的 NaTaO₃/Na₂Ta₂O₆ 复合光催化剂中, NaTaO₃ 与 Na₂Ta₂O₆ 间形成的纳米尺度异质结, 可有效促进光生电子和空穴的分离, 其析氢速率分别是相同条件下 NaTaO₃ 的 1.5 倍及 Na₂Ta₂O₆ 的 3 倍. 另外 NiO 的负载可使 NaTaO₃/Na₂Ta₂O₆ 的光解水析氢活性大幅提高, 这对钽酸盐体系光催化剂的发展具有重要意义.

参 考 文 献

- 1 Fujishima A, Honda K. *Nature*, 1972, **238**: 37

- 2 Kato H, Kudo A. *Chem Phys Lett*, 1998, **295**: 487
- 3 Kato H, Kudo A. *Catal Lett*, 1999, **58**: 153
- 4 Otsuka H, Kim K Y, Kouzu A, Takimoto I, Fujimori H, Sakata Y, Imamura H, Matsumoto T, Toda K. *Chem Lett*, 2005, **34**: 822
- 5 Xu T G, Zhao X, Zhu Y F. *J Phys Chem B*, 2006, **110**: 25825
- 6 Porob D G, Maggard P A. *J Solid State Chem*, 2006, **179**: 1727
- 7 Li D F, Zheng J, Li Z S, Fan X X, Liu L F, Zou Z G. *Int J Photoenergy*, 2007: 21860/1
- 8 Ratnamala A, Suresh G, Kumari V D, Subrahmanyam M. *Mater Chem Phys*, 2008, **110**: 176
- 9 方亮, 张辉, 鄢俊兵, 杨卫明. 物理化学学报 (Fang L, Zhang H, Yan J B, Yang W M. *Acta Phys-Chim Sin*), 2003, **19**: 82
- 10 Li Y X, Chen G, Zhang H J, Li Z H, Sun J X. *J Solid State Chem*, 2008, **181**: 2653
- 11 Zhou C, Chen G, Li Y X, Zhang H J, Pei J. *Int J Hydrogen Energy*, 2009, **34**: 2113
- 12 Miseki Y, Kato H, Kudo A. *Energy Environ Sci*, 2009, **2**: 306
- 13 Hu C-C, Tsai C-C, Teng H. *J Am Ceram Soc*, 2009, **92**: 460
- 14 Li Z H, Wang Y X, Liu J W, Chen G, Li Y X, Zhou C. *Int J Hydrogen Energy*, 2009, **34**: 147
- 15 Tian M K, Shangguan W F, Yuan J, Jiang L, Chen M X, Shi J W, Ouyang Z Y, Wang S J. *Appl Catal A*, 2006, **309**: 76
- 16 孙超, 黄浪欢, 刘应亮. 高等学校化学学报 (Sun Ch, Huang L H, Liu Y L. *Chem J Chin Univ*), 2006, **27**: 1749
- 17 Ishihara T, Baik N S, Ono N, Nishiguchi H, Takita Y. *J Photochem Photobiol A*, 2004, **167**: 149
- 18 张晓艳, 崔晓莉. 物理化学学报 (Zhang X Y, Cui X L. *Acta Phys-Chim Sin*), 2009, **25**: 1829
- 19 Lee Y G, Watanabe T, Takata T, Kondo J N, Hara M, Yoshimura M, Domen K. *Chem Mater*, 2005, **17**: 2422
- 20 Goh G K L, Levi C G, Lange F F. *J Mater Res*, 2002, **17**: 2852
- 21 Murphy C J, Jana N R. *Adv Mater*, 2002, **14**: 80
- 22 Liu J W, Chen G, Li Z H, Zhang Z G. *Int J Hydrogen Energy*, 2007, **32**: 2269
- 23 Yu Y, Yu J C, Chan C Y, Che Y K, Zhao J C, Ding L, Ge W K, Wong P K. *Appl Catal B*, 2005, **61**: 1
- 24 Yao Y, Li G H, Ciston S, Lueptow R M, Gray K A. *Environ Sci Technol*, 2008, **42**: 4952
- 25 Yen C-Y, Lin Y-F, Hung C-H, Tseng Y-H, Ma C-C M, Chang M-C, Shao H. *Nanotechnology*, 2008, **19**: 045604
- 26 Yu Y, Yu J C, Yu J G, Kwok Y-C, Che Y-K, Zhao J C, Ding L, Ge W K, Wong P-K. *Appl Catal A*, 2005, **289**: 186
- 27 郑华荣, 崔言娟, 张金水, 丁正新, 王心晨. 催化学报 (Zheng H R, Cui Y J, Zhang J Sh, Ding Zh X, Wang X Ch. *Chin J Catal*), 2011, **32**: 100
- 28 Yu J G, Hai Y, Jaroniec M. *J Colloid Interf Sci*, 2011, **357**: 223
- 29 Ren C L, Yang B F, Wu M, Xu J, Fu Z P, Lü Y, Guo T, Zhao Y X, Zhu C Q. *J Hazard Mater*, 2010, **182**: 123
- 30 Scaife D E. *Sol Energy*, 1980, **25**: 41
- 31 Arai T, Yanagida M, Konishi Y, Iwasaki Y, Sugihara H, Sayama K. *J Phys Chem C*, 2007, **111**: 7574
- 32 陈晓波. 催化学报 (Chen X B. *Chin J Catal*), 2009, **30**: 839
- 33 刘兴平, 蒋荣英, 柳松. 催化学报 (Liu X P, Jiang R Y, Liu S. *Chin J Catal*), 2010, **31**: 1381

英 译 文

English Text

Hydrogen is expected to be a new and clean energy source that will solve the energy crisis. In 1972, Fujishima et al. [1] found that a TiO₂-Pt electrode could decompose water to H₂ and O₂ at room temperature under near-UV irradiation. Since then the photocatalytic decomposition of water has been considered to be an ideal reaction to obtain hydrogen. Various semiconductor oxides such as TiO₂ have been investigated extensively as photocatalysts for water splitting. In 1998, Kudo et al. [2,3] reported that MTaO₃ exhibited fairly high activity for the photocatalytic decomposition of water under ultraviolet irradiation. In particular, the quantum efficiency reached 28% after loading NiO. Since then, various Ta-based oxides have attracted much attention such as MTaO₃ (M = Li, Na, K), M₃TaO₇ (M = Y, Yb, Gd, La), Ca₂Ta₂O₇, K₃Ta₃B₂O₁₂, MTa₂O₆ (M = Sr, Ba, Ni, Mn, Co), Bi₂MTaO₇ (M = La, Y), Ba₂LnTi₂Ta₃O₁₅ (Ln = Y, La), K₂Sr_{1.5}Ta₃O₁₀, M₂La_{2/3}Ta₂O₇ (M = H, K), A₂Bi₂Ta₂O₉ (A = Ca, Sr, Ba), M₅Ta₄O₁₅ (M = Sr, Ba), H₂SrTa₂O₇, etc. [4–15]. In a previous study, we prepared a new photocatalyst Na₂Ta₂O₆ with a special rod structure by a solid-state reaction combined hydrothermal method [16]. We found that the as-prepared Na₂Ta₂O₆ exhibited high activity.

Ishihara et al. [17] prepared K₂Ta₂O₆ with a pyrochlore structure and KTaO₃ with a perovskite structure using different methods. Their results showed that the photocatalytic activity of the obtained samples increased in the order: KTaO₃ (solid state reaction) < KTaO₃ (alkoxide reaction) << K₂Ta₂O₆ (alkoxide reaction). Ishihara pointed out that a different structure might be the main reason for the different photocatalytic activities. Sodium tantalate has two different crystal structures: NaTaO₃ with a perovskite structure and Na₂Ta₂O₆ with a pyrochlore structure. However, differences in the structure and performance between NaTaO₃ and Na₂Ta₂O₆ have not been studied systematically. Although they have the same chemical composition, their photocatalytic activity is different because of their different crystal structures.

In this paper, NaTaO₃ with a perovskite structure, Na₂Ta₂O₆ with a pyrochlore structure, and a NaTaO₃/Na₂Ta₂O₆ composite photocatalyst were synthesized using sodium carbonate, sodium stearate, and sodium acetate as precursors, respectively. The effects of different precursors on the structure of the obtained samples as well as the different structure on the photocatalytic activity for water splitting were studied systematically.

1 Experimental

1.1 Preparation of sodium tantalate

The precursor (sodium carbonate, sodium stearate, and sodium acetate) and Ta₂O₅ in a Ta/Na molar ratio of 1:3 were added to a mixture of ethylene glycol (5 ml, AR, Guangzhou Chemical Reagent Factory, China) and deionized water (25 ml). The suspension was stirred in a water bath at 80 °C for 2 h and was transferred to a 50 ml Teflon-lined stainless steel autoclave. Finally, the autoclave was maintained at 180 °C for 24 h and was then allowed to cool to room temperature naturally. After filtering, washing, and drying, sodium tantalate samples were obtained. The as-prepared samples were immersed in an aqueous Ni(NO₃)₂ solution for 4 h and then the samples were subjected to high temperature to give NiO-loaded photocatalysts.

1.2 Characterization

X-ray diffraction (XRD) patterns were obtained using MASL- XRD2 with Cu K_{α1} radiation ($\lambda = 0.154056$ nm) in a scan range 2θ between 10° and 80° at a rate of 4°/min (40 kV, 20 mA). Transmission electron microscopy (TEM) and scanning electron microscopy (SEM) were carried out using a JEOL-2100F and a PHILIPS XL-30 ESEM, respectively. The UV-Vis diffuse reflectance spectra (DRS) were collected on a Shimadzu UV-2501PC UV-Vis scanning spectrophotometer. Photoluminescence (PL) emission spectra were recorded using a Hitachi F-4500. X-ray photoelectron spectroscopy (XPS) was carried out using a ESCALAB-250 with Al K_α radiation.

1.3 Photocatalytic reaction

The experiment was carried out in a photocatalytic reaction system (CEL-HX300, Beijing Chinese Education Au-Light Co., Ltd.). The samples (0.1 g) were dispersed in a 100 ml mixture of Na₂S (0.1 mol/L) and Na₂SO₃ (0.04 mol/L), which were added as sacrificial agents because of their ability to eliminate holes [18]. After pumping nitrogen through the system for 30 min, the suspension was stirred for 6 h under continuous irradiation with a 500 W Xe lamp. A quantitative analysis of H₂ was measured using a gas chromatograph (GC9800, Shanghai Kechuang Technology Co., Ltd.).

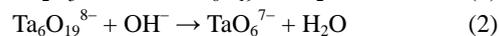
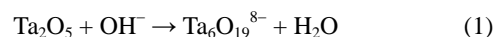
2 Results and discussion

2.1 XRD analysis

Figure 1 shows the XRD patterns of different samples.

NaTaO₃ with an ABO₃ perovskite structure was obtained when using sodium carbonate as a precursor and the lattice parameters were assigned to a monoclinic system (JCPDS 74-2477; $a = 0.3889$ nm, $b = 0.38885$ nm, $c = 0.3899$ nm, $\alpha = \gamma = 90^\circ$, $\beta = 90.367^\circ$). When sodium stearate was used as a precursor, the obtained samples were Na₂Ta₂O₆ with a pyrochlore cubic crystal structure (JCPDS 70-1155; $a = b = c = 1.044$ nm, $\alpha = \beta = \gamma = 90^\circ$). XRD patterns of the hydrothermal products that were derived from the sodium acetate precursor were different from the first two samples. The XRD peaks located at $2\theta = 22.85^\circ, 32.55^\circ, 40.23^\circ, 46.67^\circ, 52.58^\circ, 73.06^\circ, \text{ and } 77.56^\circ$ are attributed to NaTaO₃ while those located at $2\theta = 14.68^\circ, 28.32^\circ, 29.61^\circ, 34.32^\circ, 37.514^\circ, 45.08^\circ, 49.33^\circ, 51.75^\circ, 61.47^\circ, 63.58^\circ, \text{ and } 80.05^\circ$ are attributed to Na₂Ta₂O₆. It is obvious that the crystal phase is a mixed NaTaO₃ and Na₂Ta₂O₆ phase.

It has been reported that NaTaO₃ forms preferentially under higher alkaline concentrations. In contrast, Na₂Ta₂O₆ is more easily obtained under lower alkaline concentrations. The former is a metastable phase while the latter is a thermodynamically stable phase [19]. In our work, NaTaO₃ and Na₂Ta₂O₆ were obtained when sodium carbonate and sodium stearate were used as precursors, respectively. The result agrees well with that in the literature for the alkaline concentration of sodium carbonate solution was higher than that of the sodium stearate solution. However, when sodium acetate at the lowest alkaline concentration was used in this study as a precursor, a mixed phase of NaTaO₃ and Na₂Ta₂O₆ was produced. The formation of sodium tantalate is controllable by manipulating the pH and also by manipulating acid radicals. During the hydrothermal process, Ta₂O₅ was dissolved in an alkaline solution at high temperature and high pressure, resulting in octahedral TaO₆⁷⁻. The octahedral TaO₆⁷⁻ species connect to each other differently under different conditions to form a three-dimensional network. Na⁺ was positioned within the interstitial sites:



Therefore, the type of synthesized phase under hydrothermal conditions was strongly dependent on the connection of the octahedral TaO₆⁷⁻ and the migration of Na⁺. When sodium stearate was used as a precursor, C₁₆H₃₅COO⁻ with a large radius likely formed an ionic atmosphere around Na⁺. The size of Na⁺ was thus enlarged. As a result the volume of the interstitial sites that were occupied by Na⁺ increased too. Furthermore, C₁₆H₃₅COO⁻ volatilized with difficulty and consequently the transformation of metastable Na₂Ta₂O₆ to stable NaTaO₃ was restrained. Finally, Na₂Ta₂O₆ with a looser packing structure was preferentially obtained. When sodium carbonate was used as a precursor, NaTaO₃ with a compact packing of atoms was preferentially obtained. There

are two possible reasons for this result: the small radius of CO_3^{2-} and the high alkaline concentration of the sodium carbonate solution. When sodium acetate was used as a precursor, CH_3COO^- was found to be smaller than $\text{C}_{16}\text{H}_{35}\text{COO}^-$ but larger than CO_3^{2-} . Therefore, the effect of CH_3COO^- on the migration of Na^+ was higher than that of $\text{C}_{16}\text{H}_{35}\text{COO}^-$ but lower than that of CO_3^{2-} , resulting in a mixed NaTaO_3 and $\text{Na}_2\text{Ta}_2\text{O}_6$ phase.

It has been reported that high alkaline concentration is necessary to prepare the sodium tantalate by the hydrothermal method. However, in this paper sodium tantalate was synthesized at fairly low alkaline concentration, which may be attributed to the addition of ethylene glycol during the hydrothermal process. It was considered that water molecules showed strong solvent effects on OH^- due to the hydrogen bond. Therefore, in the water alone system, OH^- was shield by water molecules. As a result the actual activity of OH^- decreased. In the water/glycol system, the solvent effect of ethylene glycol on OH^- was lower than that of water on OH^- because of its large molecular volume. Therefore, the OH^- activity in the water/glycol system was higher than that in the water alone system at the same alkaline concentration. In other words, the same effect was obtained by adding ethylene glycol and increasing the alkaline concentration.

2.2 SEM and HRTEM analysis

Figure 2 shows the SEM images of different sodium tantalate samples. The NaTaO_3 obtained from the sodium carbonate precursor appeared to be irregular nanocrystalline with a particle size ranging from 500 to 600 nm. The $\text{Na}_2\text{Ta}_2\text{O}_6$ obtained from sodium stearate was composed of 200 nm particles and nanorods with a length of up to several micrometers. We previously reported the successful formation of $\text{Na}_2\text{Ta}_2\text{O}_6$ with similar nanorod morphology by hydrothermal synthesis [16]. As for $\text{NaTaO}_3/\text{Na}_2\text{Ta}_2\text{O}_6$, its morphology was found to be similar to that of NaTaO_3 except for the slight decrease in size. The average particle size of $\text{NaTaO}_3/\text{Na}_2\text{Ta}_2\text{O}_6$ was estimated to be 300 nm. Our experimental results indicate that crystal growth is strongly dependent on the type of precursor.

When using sodium carbonate as a precursor, the sodium carbonate solution gave a fairly high alkaline concentration. Ta_2O_5 dissolved quickly and thus the system soon became supersaturated. In addition, CO_3^{2-} was easily removed and had almost no effect on the following crystal growth. As a result the ripening process was sufficient and relatively large NaTaO_3 particles were obtained.

When using sodium acetate whose solution gave a low alkaline concentration as a precursor, the dissolution rate of Ta_2O_5 decreased and the system took longer to reach super-

saturation. Therefore, relatively small $\text{NaTaO}_3/\text{Na}_2\text{Ta}_2\text{O}_6$ particles were obtained. When using sodium stearate as a precursor, long chain $\text{C}_{16}\text{H}_{35}\text{COO}^-$ volatilized with difficulty. Because crystal growth must be accompanied by the removal of solvent and the formation of a chemical bond between various precursors, crystal transformation and crystal growth were inhibited. As a result relatively small $\text{Na}_2\text{Ta}_2\text{O}_6$ particles were obtained. Furthermore, some of the growth units grew along one dimension because of the template model effects of $\text{C}_{16}\text{H}_{35}\text{COO}^-$, resulting in a special rod structure. The experimental results showed that the precursor can strongly govern the crystal structure and the morphology.

To visualize the tight-contact heterojunction, $\text{NaTaO}_3/\text{Na}_2\text{Ta}_2\text{O}_6$ was investigated by HRTEM. As shown in Fig. 3, two sets of different lattice images were observed with d spaces of 0.39 and 0.30 nm, corresponding to the (100) plane of perovskite NaTaO_3 and the (222) plane of pyrochlore $\text{Na}_2\text{Ta}_2\text{O}_6$, respectively. The lattice fringes of NaTaO_3 and $\text{Na}_2\text{Ta}_2\text{O}_6$ were cut through the interface, indicating the formation of chemical bonds and heterojunctions. HRTEM analysis gave direct evidence for the interface junction between NaTaO_3 and $\text{Na}_2\text{Ta}_2\text{O}_6$ in the $\text{NaTaO}_3/\text{Na}_2\text{Ta}_2\text{O}_6$ mixed phase, which might improve the separation of electron-holes during the photocatalytic process.

2.3 UV-Vis DRS analysis

Figure 4 shows the UV-Vis diffuse reflection spectra of different samples. The bandgap was determined using the equation $E_g(\text{eV}) = 1240/\lambda(\text{nm})$, where λ is the wavelength that corresponds to the absorption band edge. The bandgaps for NaTaO_3 , $\text{Na}_2\text{Ta}_2\text{O}_6$, and $\text{NaTaO}_3/\text{Na}_2\text{Ta}_2\text{O}_6$ were found to be 4.27, 4.42, and 4.13 eV, respectively. Because the valence and conduction bands are O 2p and Ta 5d, respectively, for both NaTaO_3 and $\text{Na}_2\text{Ta}_2\text{O}_6$ [3,14,19] the differences in the bandgap can be explained by the different types of overlap of the atomic orbitals of tantalum and oxygen. The average Ta–O distance is 197.8 pm in NaTaO_3 while that in $\text{Na}_2\text{Ta}_2\text{O}_6$ is 199.3 pm. Because $\text{Na}_2\text{Ta}_2\text{O}_6$ has a longer Ta–O distance than that in NaTaO_3 , the energy of the conduction band is higher for $\text{Na}_2\text{Ta}_2\text{O}_6$. The bandgap of $\text{NaTaO}_3/\text{Na}_2\text{Ta}_2\text{O}_6$ is much smaller than those of NaTaO_3 and $\text{Na}_2\text{Ta}_2\text{O}_6$. This is possibly due to the distorted crystal structure. Although NaTaO_3 and $\text{Na}_2\text{Ta}_2\text{O}_6$ had the same chemical composition, the method of connection between the TaO_6 octahedra is different. The crystal structure of NaTaO_3 was found to be a perovskite structure while that of $\text{Na}_2\text{Ta}_2\text{O}_6$ was found to be a pyrochlore structure. The TaO_6 octahedral was greatly distorted when an interface heterojunction formed between the $\text{NaTaO}_3/\text{Na}_2\text{Ta}_2\text{O}_6$ particles. DRS results suggest that the crystal structure should influence their band structure although specific details are not known at present.

2.4 PL analysis

Figure 5 shows PL spectra of the different samples. PL is an efficient way to study the migration and trapping of charge carriers and the transfer efficiency and electron-hole recombination in semiconductors. The PL signals are attributed to the radiative recombination process of self-trapped excitons [23–27]. Therefore, the decrease in PL intensity indicates an enhancement in the separation efficiency of the electron-hole pairs. From Fig. 5 we can see that the PL peaks of the different samples are all located at 550 nm. This indicates that the change in crystal structure did not cause any new luminescence. The PL intensity increased as in the order $\text{Na}_2\text{Ta}_2\text{O}_6 > \text{NaTaO}_3 > \text{NaTaO}_3/\text{Na}_2\text{Ta}_2\text{O}_6$. The PL signals of $\text{NaTaO}_3/\text{Na}_2\text{Ta}_2\text{O}_6$ were far lower than those of NaTaO_3 and $\text{Na}_2\text{Ta}_2\text{O}_6$, indicating the lowest electron-hole recombination rate and the highest quantum efficiency. Previous studies [28,29] showed that the order of photocatalytic activity was opposite to that of PL intensity. Our photocatalytic results agree well with that in the literature.

2.5 XPS analysis

Table 1 summarizes the XPS data showing the binding energy of O 1s and Ta 4f_{7/2} for different samples. The TaO_6^{7-} in $\text{Na}_2\text{Ta}_2\text{O}_6$ was greatly distorted and oxygen atoms were regularly missing from the ideal structure. Therefore, quasi-free electrons might form and maintain the electrical neutrality. Consequently, Ta^{5+} accepted electrons resulting in an increased electron density as well as increased shielding effects. As a result the O 1s and Ta 4f_{7/2} binding energies for $\text{Na}_2\text{Ta}_2\text{O}_6$ were lower than those of NaTaO_3 . For $\text{NaTaO}_3/\text{Na}_2\text{Ta}_2\text{O}_6$, the heterojunction that formed at the interface between NaTaO_3 and $\text{Na}_2\text{Ta}_2\text{O}_6$ might become an electron transfer channel (electrons transferred from $\text{Na}_2\text{Ta}_2\text{O}_6$ to NaTaO_3). The electron density and the shielding effect decreased. Therefore, the O 1s and Ta 4f_{7/2} binding energies for $\text{NaTaO}_3/\text{Na}_2\text{Ta}_2\text{O}_6$ lay between those of NaTaO_3 and $\text{Na}_2\text{Ta}_2\text{O}_6$.

2.6 Photocatalytic activity analysis

Figure 6 shows the photocatalytic activity for H₂ evolution from a water- Na_2S - Na_2SO_3 mixture. As shown, there was no appreciable decrease in gas evolution during irradiation. The activity of $\text{NaTaO}_3/\text{Na}_2\text{Ta}_2\text{O}_6$ was much higher than those of NaTaO_3 and $\text{Na}_2\text{Ta}_2\text{O}_6$. The rate of H₂ evolution for $\text{NaTaO}_3/\text{Na}_2\text{Ta}_2\text{O}_6$ reached 49 $\mu\text{mol/h}$, which was 1.5 times that of NaTaO_3 and 3 times that of $\text{Na}_2\text{Ta}_2\text{O}_6$. According to the PL measurements and the photocatalysis results, it could be

concluded that the photocatalytic activity was mainly controlled by the charge separation efficiency. This can be explained as follows: the heterojunction that exists at the interface of the mixed phase promotes charge separation.

Scaife [30] used the equation of $V_{\text{fb}}(\text{NHE}) = 2.94 - E_{\text{g}}$ to calculate the flat potential, where V_{fb} was the flat potential. Since the Fermi level was approximately equal to the flat potential, the Fermi levels were -1.33 eV for NaTaO_3 , -1.48 eV for $\text{Na}_2\text{Ta}_2\text{O}_6$, and -1.18 eV for $\text{NaTaO}_3/\text{Na}_2\text{Ta}_2\text{O}_6$. The Fermi level of $\text{Na}_2\text{Ta}_2\text{O}_6$ was 0.22 eV higher than that of NaTaO_3 . Therefore, the electrons would transfer from $\text{Na}_2\text{Ta}_2\text{O}_6$ to NaTaO_3 through their interface when nanoparticles with different phases connected to form heterojunctions [31–33]. A built-in electric field forms with an orientation from $\text{Na}_2\text{Ta}_2\text{O}_6$ to NaTaO_3 in the mixed $\text{NaTaO}_3/\text{Na}_2\text{Ta}_2\text{O}_6$ phase. Therefore, when $\text{NaTaO}_3/\text{Na}_2\text{Ta}_2\text{O}_6$ is illuminated by UV light a transfer of photogenerated electrons from NaTaO_3 to $\text{Na}_2\text{Ta}_2\text{O}_6$ occurs, which is driven by the electric field at the interface and the recombination of photogenerated electron-hole pairs is significantly reduced, which enhances the photocatalytic activity. Further experimental results indicate that the H₂ evolution rate of $\text{NaTaO}_3/\text{Na}_2\text{Ta}_2\text{O}_6$ after loading with 2.5% NiO increased by a factor of 1.4. To obtain higher activity, a further investigation into NiO loading is required.

It should be noted that the bandgap and the high potential of the conduction band is advantageous for water splitting. However, in this paper the photocatalytic activity for H₂ evolution does not correlate with the bandgap results. This indicates that the band structure is not an important factor for sodium tantalate during H₂O photocatalytic decomposition.

3 Conclusions

The structure and photocatalytic activity of different sodium tantalate compounds that were obtained from different precursors were studied. The effects of the sodium precursor on the crystalline structure and morphology are discussed. The separation efficiency of the electron-hole pairs is an important factor that affects the photocatalytic activity. The heterojunction that formed within $\text{NaTaO}_3/\text{Na}_2\text{Ta}_2\text{O}_6$ promotes the separation of electron-hole pairs. The hydrogen evolution rate of the $\text{NaTaO}_3/\text{Na}_2\text{Ta}_2\text{O}_6$ composite photocatalyst was 1.5 times that of NaTaO_3 and 3 times that of $\text{Na}_2\text{Ta}_2\text{O}_6$ under the same conditions. In addition, loading with NiO greatly improves the photocatalytic activity for H₂ evolution from water.

Full-text paper available online at Elsevier ScienceDirect
<http://www.sciencedirect.com/science/journal/18722067>